Numerical simulation of bond degradation subjected to corrosion-induced crack by simplified rebar and interface model using RBSM

Yizhou Yang (Corresponding author)

Ph.D.

Department of Civil and Environmental Engineering

Nagoya University

Furo-cho, Chikusa-ku, Nagoya, 464-8603, Japan

yyz1991@hotmail.com

Hikaru Nakamura

Professor

Department of Civil and Environmental Engineering

Nagoya University

Furo-cho, Chikusa-ku, Nagoya, 464-8603, Japan

hikaru@cc.nagoya-u.ac.jp

Yoshihito Yamamoto

Associate Professor

Department of Civil and Environmental Engineering

Nagoya University

Furo-cho, Chikusa-ku, Nagoya, 464-8603, Japan

y.yamamoto@civil.nagoya-u.ac.jp

Taito Miura

Assistant Professor

Department of Civil and Environmental Engineering
Nagoya University
Furo-cho, Chikusa-ku, Nagoya, 464-8603, Japan
t.miura@civil.nagoya-u.ac.jp

Abstract

The bond degradation subjected to corrosion-induced crack was investigated numerically using 3D Rigid Body Spring Model (RBSM) in which rebar was modeled by solid elements without modeling explicitly the details of rebar ribs. The proposed numerical model considers both corrosion expansion and shear stress transfer behavior through the interface elements. Validation of proposed model showed that it is possible to obtain reasonable bond performance of non-corroded specimen as meso-scale models. By comparison with experimental results, the proposed model was verified to reproduce the bond deterioration considering corrosion-induced crack with different concrete cover thickness. Moreover, bond deterioration mechanism subjected to corrosion-induced crack was clarified through the crack development and stress distribution of concrete and was found to be the combined effects of degradation of the compressive stress in diagonal compression struts and ring-tension around rebar. Bond deterioration of specimen with larger concrete cover is more sensitive to formation of corrosion crack.

Keywords

Bond-slip relationship, corrosion-induced crack, concrete cover, surface crack width, bond deterioration mechanism, 3D RBSM

1 Introduction

Numerical method is a powerful and efficient tool to estimate the behavior of reinforced concrete (RC) member subjected to corrosion. As one of the critical components in corrosion-induced degradation of the aged RC structure, bond deterioration between rebar and concrete will directly affect the load-carrying ability and ductility [1-4]. Since bond behavior is a complex interaction between cracked concrete and rusted rebar, the numerical method of bond evaluation is of great importance.

Based on the recent experimental study on individual effects including corrosion-induced crack, corroded rebar shape and rust accumulation on bond deterioration conducted by Yang et al. [5], corrosion-induced crack is confirmed to be the dominant factor influencing bond behavior. Thus, in order to interpret the effects of internal corrosion-induced cracks on the bond of rebar in RC member, a model considering the influences of rebar position and various corrosion-induced crack patterns is expected to be developed.

Characteristic of corrosion-induced crack is known to be closely related to the concrete cover thickness, rebar diameter and rebar arrangement in RC member. The cracking criterion induced by corrosion was theoretically studied. Bazant [6] suggested that cracking modes consisting of spalling mode and delamination mode are governed by both concrete cover C and the rebar spacing S. Tsutsumi et al. [7] also presented a criterion of coefficient k as a function of concrete cover C and diameter of rebar D to represent two types of internal crack patterns as shown in Figure 1. Experimental studies basing on accelerated corrosion test in laboratory [8-11] also suggested the strong correlation between internal crack pattern and rebar position embedded in concrete. Development of surface crack width corresponding to corrosion degree is also reported to be influenced by concrete cover thickness [12,13].

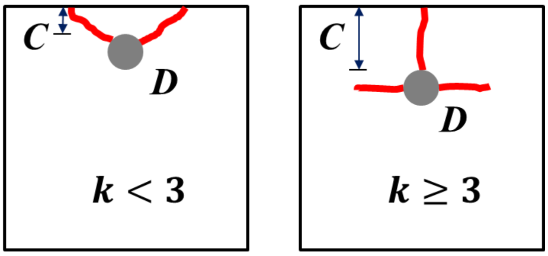

$$k = \frac{2C + D}{D}$$

Figure 1 Criterion for internal crack pattern by Tsutsumi et al. [7]

There are a couple of numerical models based on finite element method (FEM) proposed to simulate bond deterioration due to corrosion. Lee et al. [14] conducted pullout analysis of deformed rebar modeled by 2D element. 1mm thick interface elements were applied to model the bond property. The bond degradation due to corrosion was simulated by adjusting the maximum bond strength and bond rigidity obtained from test results, while cracking of concrete was not considered. Lundgren [15] proposed a 3D FEM model where deformed rebar was modeled in round shape with solid elements. In between of rebar and concrete, one corrosion layer describes uniform volume expansion of corrosion products and one interface layer describes the normal and shear forces between rebar and concrete. Parameters relating to the mechanical behavior of rust and interface layer were calibrated based on various rebar type, rebar diameter, compressive strength and concrete cover. Numerical results showed good correlation with experiments. Berra et al. [16] developed a numerical bond model considering the effect of transverse confinement on bond strength. A 3D rebar with detailed ribs was modeled to reproduce the interaction between deformed rebar and concrete, while corroded rebar shape was not considered. Concrete crack induced by corrosion expansion is simulated based on corrosion amount. Without considering the corrosion expansion, Amleh and Ghosh [17] modeled deformed rebar in round shape with solid elements and directly adopted the contact pressure and friction coefficient based on experimental results of corroded rebar to simulate the interactive forces at steel-concrete interface. In recent researches, numerical methods for bond evaluation were further developed to simulate more realistic corrosion process in rebar and concrete. Hanjari et al. [18] extended the corrosion model proposed previously by Lundgren [15,19] to consider non-uniform corrosion expansion and multi-rebar corrosion, while bond model remained consistent. Ozbolt et al. [20] established numerical model consist of deformed rebar modeled in round shape with solid elements and one-dimensional contact elements at the interface simulating both corrosion expansion and bond behavior. In the contact elements, corrosion was modeled as chemo-hygro-thermo process in radial component and bond behavior in axial component is governed by bond-slip constitutive law calibrated from experimental measurement. Numerical results suggested the dependency of bond degradation on surface crack width and the influences of concrete cover, rebar diameter and corrosion distribution. Most recently, Jiradilok et al. [21,22] performed bond analysis with discrete meso-scale element model based on 3D RBSM. Deformed rebar was modeled with detailed transverse ribs. Modification of shear and normal springs at rebar-concrete interface was calibrated from test results after corrosion expansion analysis, as an attempt to accurately simulate total effects of rebar surface condition and concrete cracking on bond deterioration and bearing capacity of corroded members.

So far these bond models of deformed rebar and concrete are including either too many complex calibrated parameters or deformed rebar shape that need to be explicitly modeled with significant number of solid elements and sophisticated mesh sizes. In addition, mechanism of bond deterioration induced by corrosion crack and its influential parameters has not been fully clarified from numerical studies. Therefore, a more simplified and concise numerical model with the consistent accuracy is required to perform parametric studies based on large number of influential factors.

In this study, the effect of corrosion-induced crack on deterioration mechanism of ultimate bond strength was investigated by a numerical method based on 3D RBSM. A three-layered RBSM model consisting concrete, rebar and interface elements were developed to simulate bond-slip behavior between deformed rebar and cracked concrete due to corrosion. The important feature of the proposed method is that deformed rebar is simplified into round rebar shape with the arrangement of concise shear transfer model at concrete-rebar interface elements, combined with concrete cracking simulation by rebar corrosion. The proposed model was first validated by experimental and meso-scale results through simulating the non-corroded bond behavior with various concrete cover thickness and compressive strength. In addition, the applicability of the model to simulate the bond deterioration caused by corrosion-induced crack subjected to concrete cover thickness was verified and bond deterioration mechanism was clarified with crack development and stress distribution in concrete.

2 Bond behavior of corroded rebar with various concrete cover by experiment

The bond-slip relationship of corroded rebar with 30mm concrete cover was experimentally investigated by Yang et al. [5]. In addition to 30mm case, specimens with larger range of concrete covers were also studied, of which 15 and 50mm cases are presented in the latter part in this study as new test results. The outline of test specimen as shown in Figure 2 is a concrete cube with 150mm side length and a high-strength D16 rebar embedded at 15, 30, 50mm concrete vertical cover and 67mm side cover. The objective concrete strength was 40MPa. Specimens were first corroded by accelerated corrosion test up to 15% corrosion. Surface crack width induced by corrosion expansion was measured based on the averaged crack width on specimen surface with minimum concrete cover (see Figure 3(a)). Cross-sectional crack induced by corrosion expansion was measured from the identical specimens prepared in the same corrosion series (see Figure 3(b)), meanwhile crack pattern after rebar pulled out was also measured. The details of experiment setup, measurement of bond stress and surface crack opening along rebar pull-out were introduced in the reference [5]. Test results are compared together with numerical analysis in section 4.

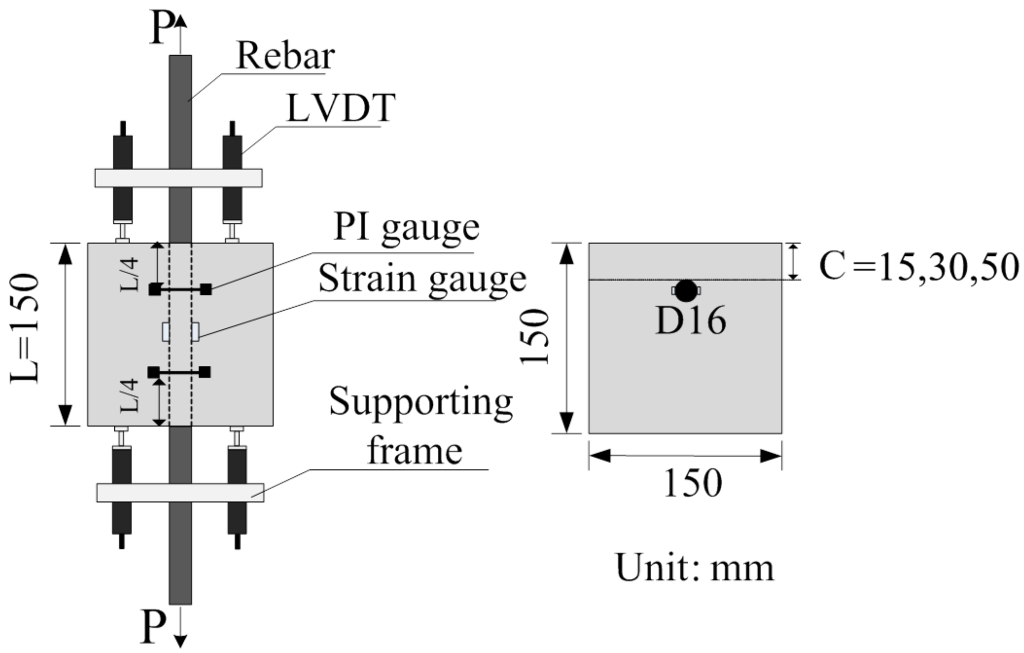

Figure 2 Outline of two end pull-out specimen

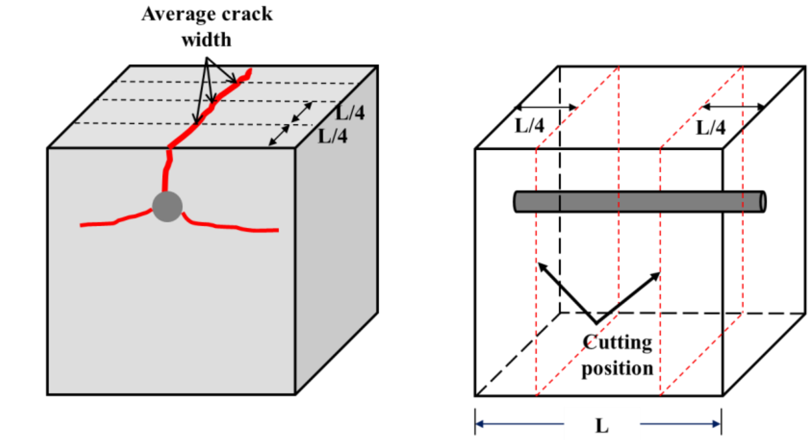

(a) Surface crack width induced by corrosion

(b) Internal crack measurement after corrosion or pull-out test

Figure 3 Diagram of surface and internal crack measurement

3 Numerical model of two end pull-out specimen

3.1 Numerical method

3D RBSM was adopted in the present numerical analysis. RBSM is one of the discrete numerical methods to represent a continuum material as an assemblage of rigid particles interconnected by zero-length springs along their boundaries as shown in Figure 4. The Voronoi diagram is applied to randomly generate the particle elements, which have six degrees of freedom at element centroids. The boundary between two adjacent elements is divided into triangles that are formed by the center of gravity and vertices of the boundary. There are three springs set at the center of each formed triangle, one normal spring and two shear springs. The advantage of this method is that the crack width can be automatically calculated as the relative displacement between centers of adjacent particles [23].

The applicability of 3D RBSM in the study of crack propagation induced by rebar corrosion have been investigated in [10-11,24-26] with the special focus on corrosion-induced cracking evolution considering various corrosion parameters. The three-layered RBSM model studying corrosion-induced crack consisted of rebar, concrete and corrosion layer. The corrosion expansion was introduced to the normal springs between the corrosion layer and rebar elements, whereas the stiffness of shear springs was neglected in previous studies. This three-layered model is adopted in the proposed numerical model as shown in Figure 5. The important features of the proposed model for bond behavior are: firstly the complex geometry of deformed rebar is simplified by the concise round rebar neglecting the detailed rebar ribs and modeled by RBSM elements with regular mesh; secondly, different from previous RBSM models, shear constitutive model is introduced to the shear springs arranged between rebar and interface element, which is modeled by the single element parallel to the circumferential direction of the rebar with thickness of 1.0 mm. The element meshing of the model is similar to the corrosion layer in the previous corrosion-induced crack simulations by Tran et al. [24] and Qiao et al. [11,25].

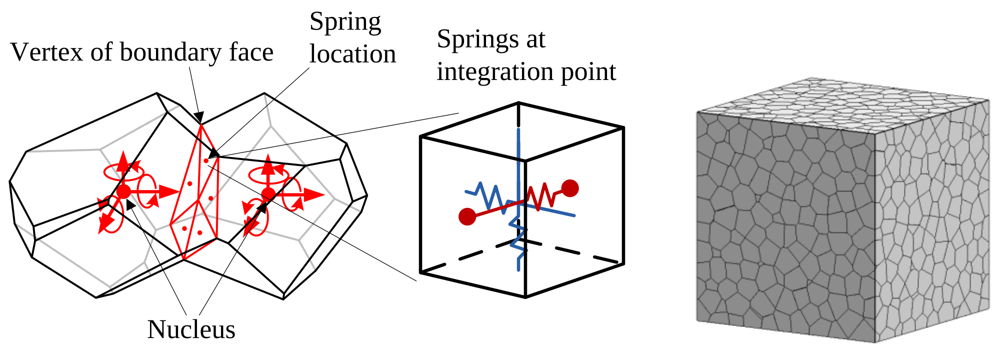

(a) Rigid-Body-Spring-Model (b) Voronoi diagram

Figure 4 Rigid Body Spring Method

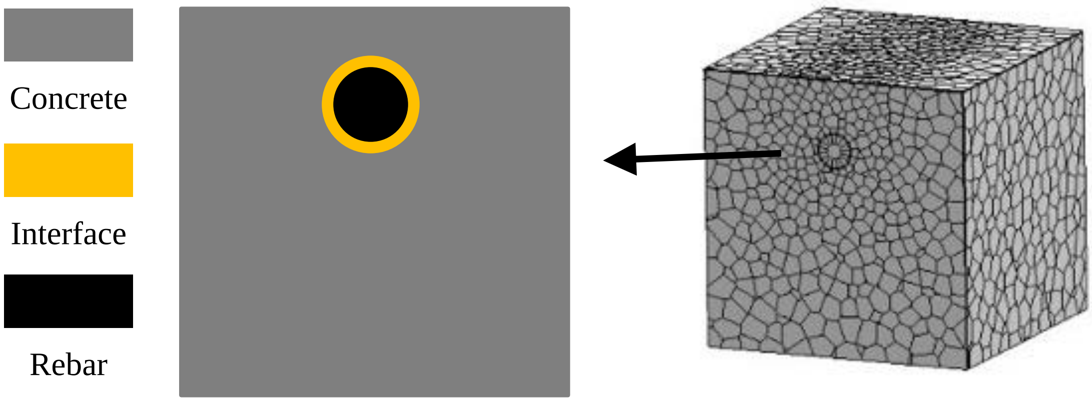

Figure 5 Diagram of numerical model

3.2 Material model

3.2.1 Concrete and rebar

The concrete material model applied in this analysis is summarized in Figure 6. Tensile and compressive models are introduced into normal springs, where f_t represents tensile strength, h is the perpendicular distance (with respect to the bounding plane) between centroids of the elements, G_F is the tensile fracture energy, f'_c compressive strength, G_{Fc} compressive fracture energy and E Young's modulus of concrete. Shear model is introduced into shear springs, in which the shear strength is assumed to follow the Mohr-Coulomb type yield criterion with the tension and compression caps. The shear transferring capacity at the cracked interface due to rebar corrosion changes according to crack opening. This effect is considered by reducing the shear modulus G using a function of the strain normal to the crack, known as shear degradation model. Material model of rebar is modeled as perfect elasto-plastic in normal springs with the Young's modulus E_s of 193000MPa and yield stress f_y of 721MPa obtained from experiments in [5].

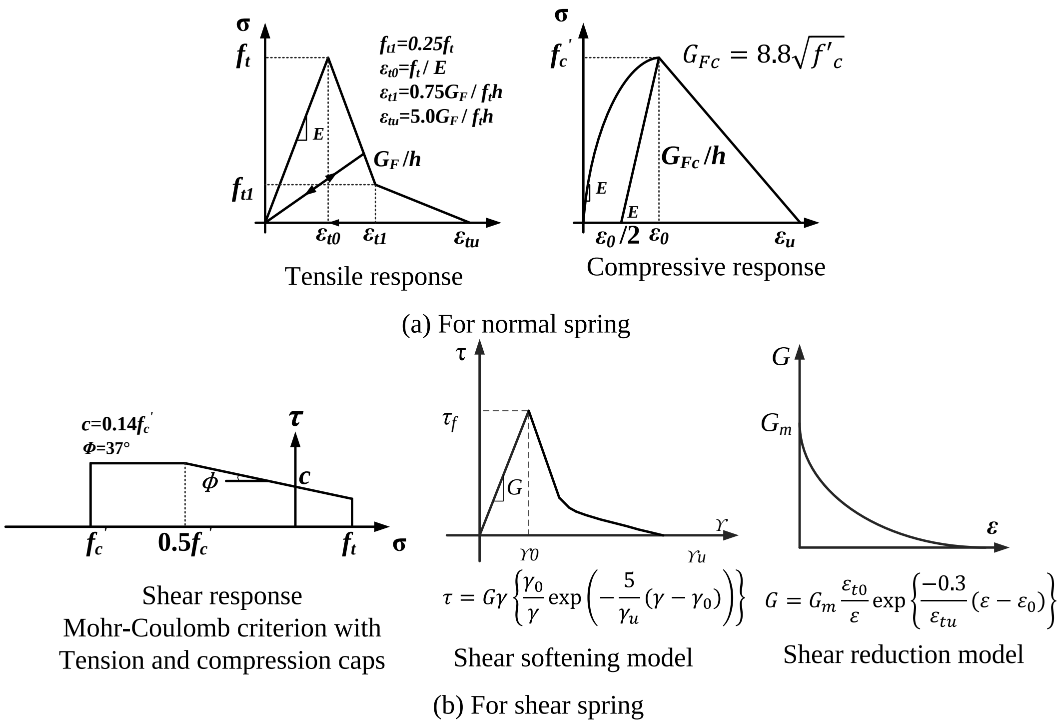

Figure 6 Concrete material constitutive model

3.2.2 Interface

Similar to concrete and rebar elements, the normal springs and shear springs are arranged at interface elements. Normal springs are arranged in the direction perpendicular to rebar surface, of which applied not only same corrosion expansion model but also same Young's modulus of 500MPa as the previous corrosion crack simulation studies [11,24,25]. Hence, simulation accuracy of the present model for corrosion-induced crack propagation is consistent.

In an attempt to simulate shear transferring mechanism induced by interlocking action between rebar ribs and concrete in the actual condition, shear springs were introduced between the interface element and rebar element in the direction parallel to rebar axis. The arrangement of shear springs between two concrete elements represents the shear mechanism of cracked concrete, which is derived from interlocking of coarse aggregate.

Meanwhile, bond stress of deformed rebar is proposed by means of Mohr-Coulomb equation in literatures [27-29] to consider the contribution of concrete confinement to the rebar, which is conceptually same as shear constitutive model of concrete. Therefore, same shear model is given to springs in both concrete and interface elements for the similarity. Parametric study regarding the shear modulus G, cohesion c and friction angle φ of shear springs at interface elements was conducted for a wide range of concrete cover thickness and compressive strength. As a result, the shear modulus G of interface springs is chosen to be much smaller than the one of concrete to define the difference in shear stiffness, while parameters related to Mohr-Coulomb criterion is consistent with concrete.

The modeling accuracy of bond behavior in this study is not necessary to be the same as experiment; instead, a simplified rebar model is developed to evaluate the influence of corrosion-induced crack quantitatively. Considering the conciseness and applicability, the constitutive model of concrete is directly adapted to the interface elements, of which only initial modulus of normal spring and shear spring were adjusted according to Table 1.

Table 1 Material parameters for normal and shear spring at concrete and interface

Element	E (MPa)	G (MPa)	c (MPa)	φ (°)	f'_c (MPa)	f_t (MPa)	G_F (N/mm)	γ_u
Concrete	30000	9000	$0.14f'_c$	37	40.0	2.69	0.11	0.015
Interface	500	250						

3.3 Validation of bond behavior of non-corroded specimen

Based on the proposed numerical model, validation of the model to reproduce the bond behavior of a deformed rebar was conducted. According to previous researches and design codes, bond behavior of non-corroded rebar is influenced by concrete cover thickness and concrete strength [30-32]. Hence, the validity of estimating the effect of concrete cover and concrete strength on bond-slip relationship by the proposed model is discussed. The objective specimens are two end pull-out specimens in the experiment study by Iizuka et al. [32]. The specimens' dimensions are shown in Figure 2 and all experiment parameters are presented in Table 2.

Table 2 Test series and parameters of specimens for validation [32]

Series	Rebar diameter D (mm)	Concrete cover C (mm)	C/D	Compressive strength (MPa)
Concrete cover	25	10	0.4	25.1
		30	1.2	25.1
		50	2.0	25.1
Compressive strength		30	1.2	11.2
				16.3
				28.0
				32.7
				41.3
				46.8
				55.8

Figure 7 shows the dimension and meshing of the specimens used in validation. As shown in Figure 7(a), for proposed model, regular mesh of 5mm is applied for the round rebar without detailed transverse ribs. Meanwhile, mesh sizes of Voronoi particles are arranged 5mm in concrete cover and around rebar and 10mm in other area. The number of solid elements is approximately 9000. In comparison, the meso-scale model with detailed rib shape presented by Ikuma et al. [33] who applied same computational program of RBSM is shown in Figure 7(b), in which a finer mesh size of rebar elements and adjacent concrete elements is recommended to be around 1-2mm which is no larger than the transverse rib height. Thus significant number of elements of 22000 is required with the meso-scale model and therefore computational time and cost is high. As compare to the meso-scale model by Jiradilok et al. [21,22] using regular mesh of deformed rebar and adjacent concrete, an average 10-20mm was used for concrete elements, the total number of elements shows similarity to the proposed model but specific manner of meshing is required in the area near to the rebar ribs. Comparably, conciseness and computational efficiency of the simplified round rebar model is demonstrated.

Consistent boundary conditions as two end pull-out test in Figure 2 are performed in analysis. For one end of rebar, the degrees of freedom of nodes on the rebar surface are fixed; for another end, incremental displacement of 0.01mm at each analytical step along axis direction is assigned. Average bond stress is calculated based on the assumed linear stress distribution within the loading-end and center points of rebar. Rebar slip is directly measured by the relative displacement between rebar ends and concrete body.

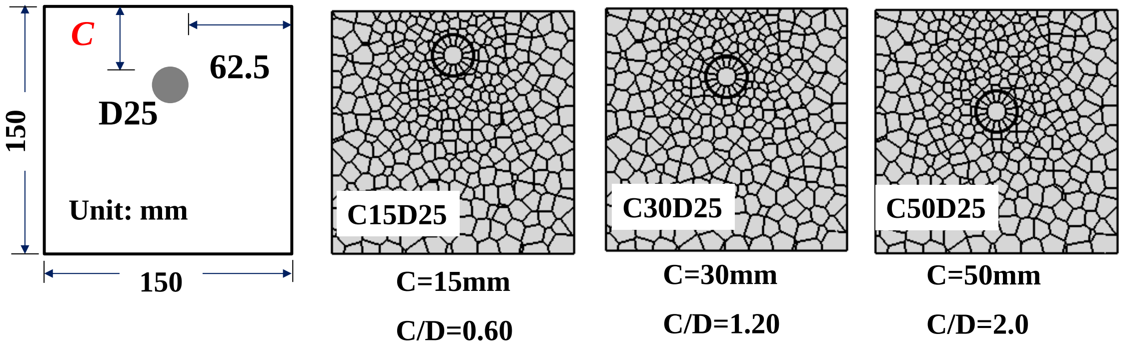

(a) Mesh of proposed simplified model

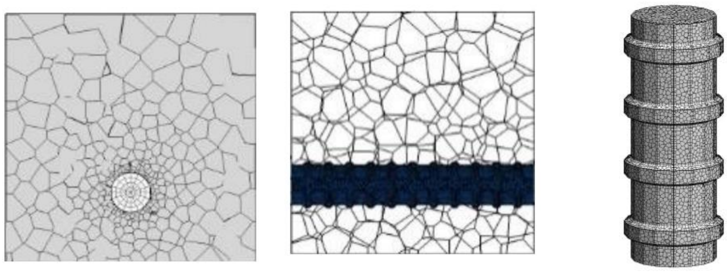

(b) Mesh of mesoscale model (Ikuma et al. [33])

Figure 7 Dimension and mesh of specimen for validation

3.3.1 Effect of concrete cover thickness

Ikuma et al. [33] modeled the detailed rebar ribs using 3D RBSM based meso-scale simulation method which is able to automatically evaluate the effect of cover thickness with the consistent interface material models as concrete. It is because that effect of concrete cover is contributed by the confinement stress around rebar near concrete cover rather than influenced by the shear constitutive model at interface. Therefore, the important feature of the proposed numerical model is the validity of simulating cover thickness effect with the material parameters adopted to interface elements in Table 1.
Figure 8 shows the comparison of bond-slip relationships under 10, 30, 50mm cover thickness between the proposed numerical model, meso-scale model and experiment. For all cover thickness cases, ultimate bond strength and slip at ultimate bond strength

by the proposed model shows better correlation with experiment than the meso-scale simulation. In addition, although initial stiffness and ductility at softening stage by proposed model shows some degree of variation with test results, the differences with meso-scale simulation is very marginal.

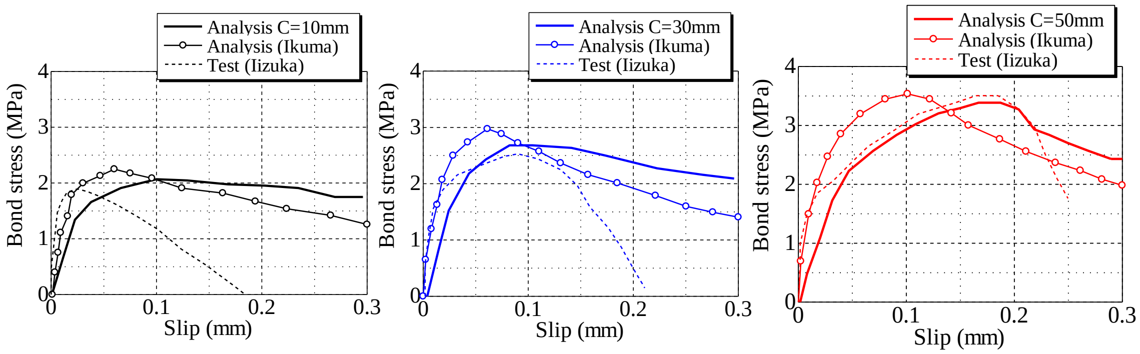

(a) C=10mm (b) C=30mm (c) C=50mm

Figure 8 Effect of cover thickness on bond-slip relationship

Surface and internal crack propagation at 0.15mm slip are shown and compared with meso-scale simulation in Figure 9. Around ultimate bond stage, development of conical crack (Goto's crack [34]) due to the bearing mechanism between deformed rib and concrete from rebar ends towards rebar center and concrete cover can be clearly observed, together with the propagation of longitude ring-tension crack from rebar ends. Comparing to the meso-scale model, although fewer diagonal crack and marginally larger crack width is observed in this simplified model, the occurrence of ring-tension, Goto's cracks and crack distribution can be rationally simulated.

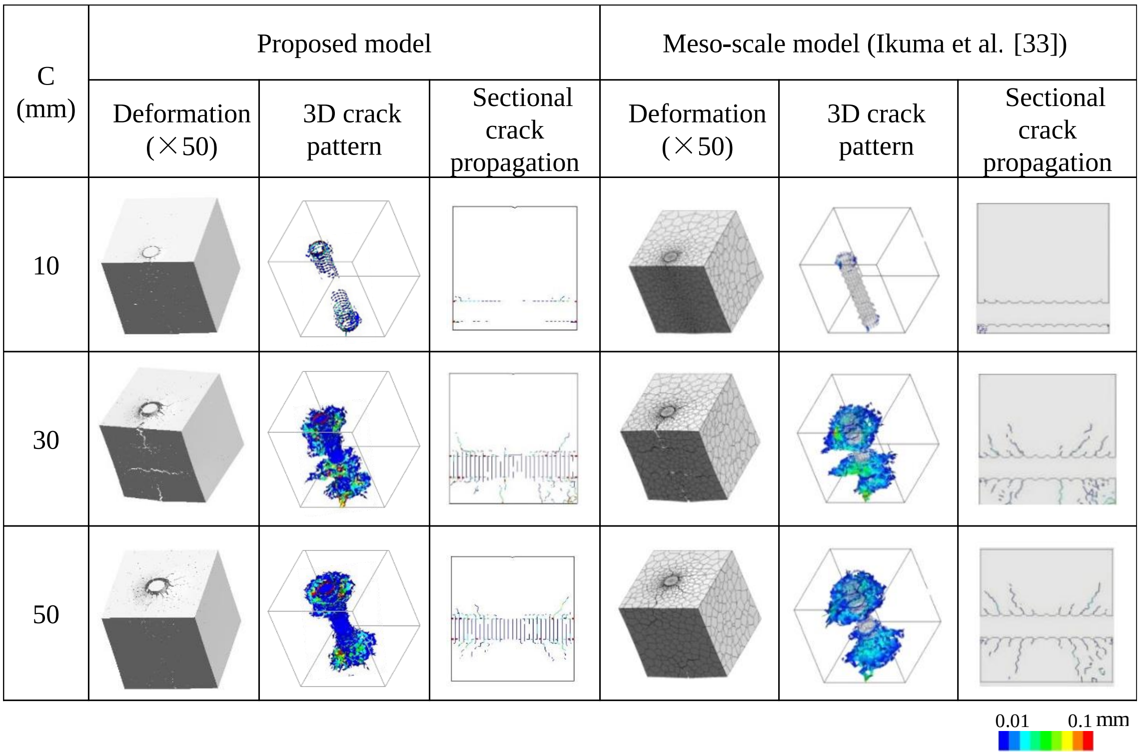

Figure 9 Surface and internal crack propagation by proposed model and meso-scale simulation (slip=0.15mm)

3.3.2 Effect of C/D ratio and concrete strength

Figure 10 shows the effect of C/D ratio on ultimate bond strength of the non-corroded specimens with various rebar diameters obtained by numerical model. Good correlation is shown among all results with the regression model proposed by Iizuka et al. [32]. Meanwhile, the smaller bond strength with larger rebar diameter has also been confirmed in the experiment which is explained by the larger bursting force generated between larger diameter rebar and concrete in the experiment.

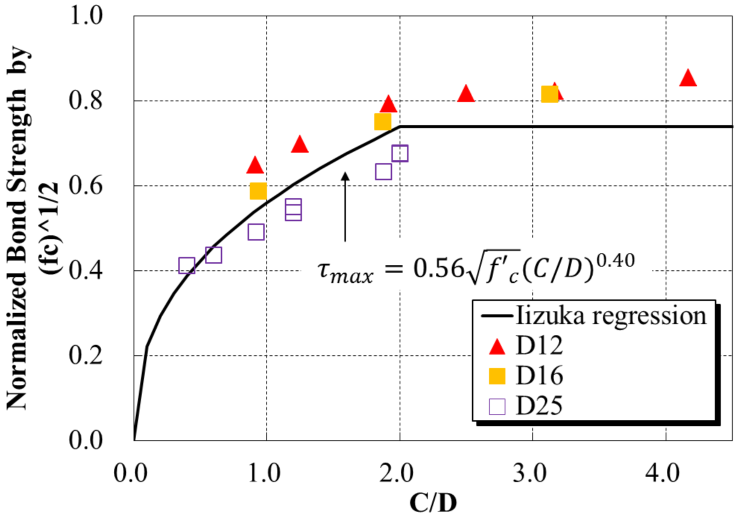

Figure 10 Effect of C/D ratio on ultimate bond strength normalized by square root of *f'c*

The validity of numerical model in simulating the effect of concrete compressive strength was also examined. In Figure 11(a), with the increase of concrete strength, a clear increase of both ultimate bond strength and slip at ultimate bond strength can be obtained, which coincide with test results. Moreover, the dependency of ultimate bond strength on concrete compressive strength shows good correlation with the regression function from the experiment (Figure 11(b)).

Therefore, the proposed numerical model is confirmed to reasonably simulate bond behavior for both effects of cover thickness, rebar diameter and concrete strength. Moreover, numerical results show the same tendency with the results of meso-scale analysis for not only bond stress–slip relationship but also the simulation of internal crack propagation.

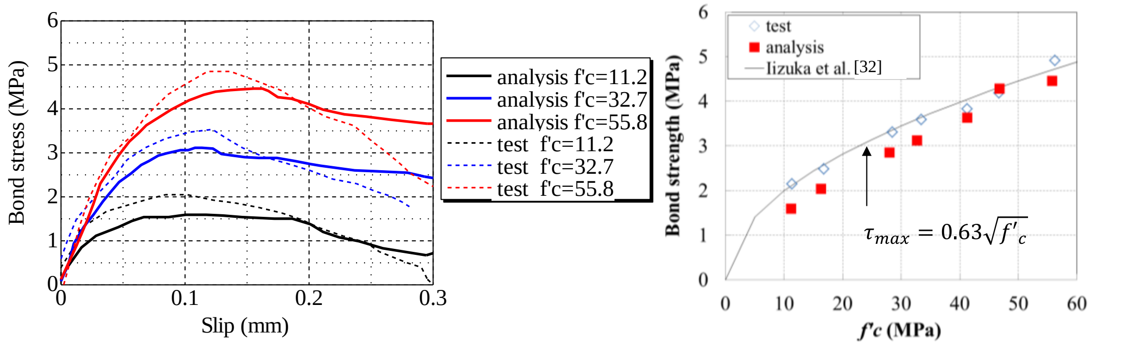

(a) Bond-slip relationship (b) Ultimate bond strength-f'_c relationship

Figure 11 Effect of concrete compressive strength on bond behavior

4 Validation of numerical model for bond behavior of two end pull-out specimens with corrosion-induced crack

Based on the performance of the proposed numerical model in simulating non-corroded specimen, validation of proposed model considering the influence of corrosion-induced crack on bond behavior was conducted. In the simulation of corroded specimen, the first analytical step is to apply the corrosion expansion. The method of corrosion expansion step adopted herein is same as described in the literatures [11,24], of which expansion of corrosion product is introduced by the initial strain at each analytical step, based on the assumed corrosion amount. The degrees of freedom of nodes at two ends of rebar are fixed during the corrosion step. As corrosion step complete, incremental displacement is applied to rebar loading-end as introduced in section 3.3. Bond-slip relationship and crack propagation of specimens with various concrete cover by the proposed model are demonstrated and compared with test results measured in section 2.

4.1 Bond-slip relationship

Bond-slip relationships subjected to various corrosion degree and concrete cover are demonstrated in Figures 12-14. In order to compare with experimental results, bond stress is normalized by square root of concrete compressive strength. As can be seen, for non-corroded specimen, numerical ultimate bond strength and corresponding slip increase with the concrete cover, which is well correlated to test results. Regardless of concrete cover, as corrosion degree increases, initial stiffness, ultimate bond strength and softening gradient deteriorates gradually. Effect of corrosion-induced crack indicates similar tendency with the findings of effect of pre-existing longitude cracks on bond behavior by Desnerck et al. [35]. Comparably, experimental bond-slip relationships indicate increase of ultimate bond strength with small corrosion degree and drastic degradation afterwards, accompanying with the general degradation of both initial stiffness and softening gradients. The differences between simulation and experiment come from neglecting the effects of corroded rebar shape and rust accumulation. Experimental study conducted by Yang et al. [5] indicated the corroded rebar surface with rust alone would cause a more than 25% increase of bond strength at 4-5% corrosion and 25% reduction of bond with 10% corrosion. Hence corrosion-induced crack was confirmed to play a dominant role which contributes to more than 50% of bond reduction at large corrosion degree and improved ductility, which is captured by simulation in Figures 12-14.

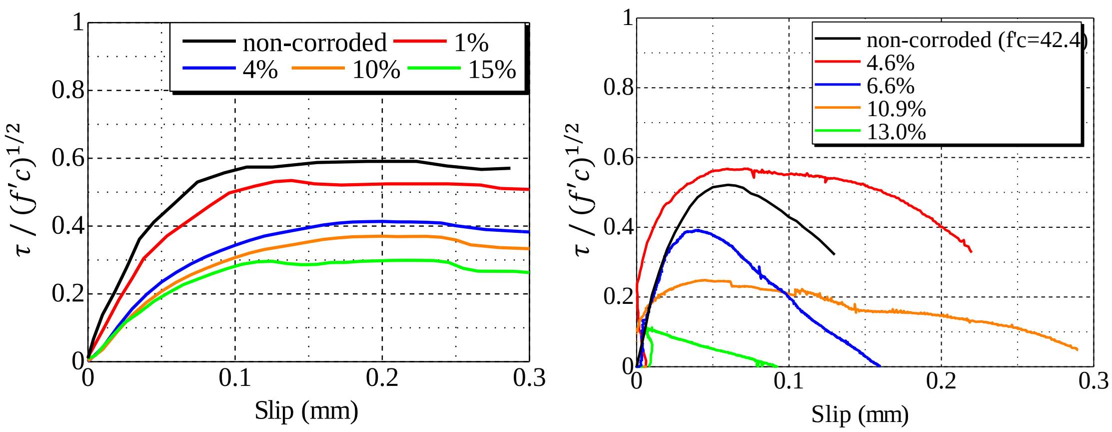

(a) Analysis (b) Experiment

Figure 12 Bond-slip relationship subjected to corrosion of C15 specimen

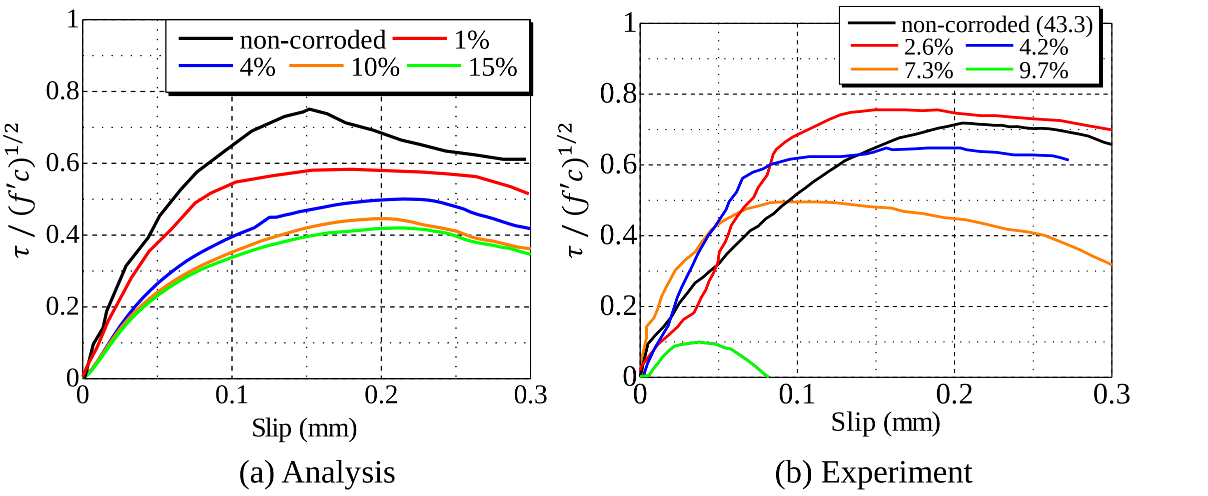

Figure 13 Bond-slip relationship subjected to corrosion of C30 specimen

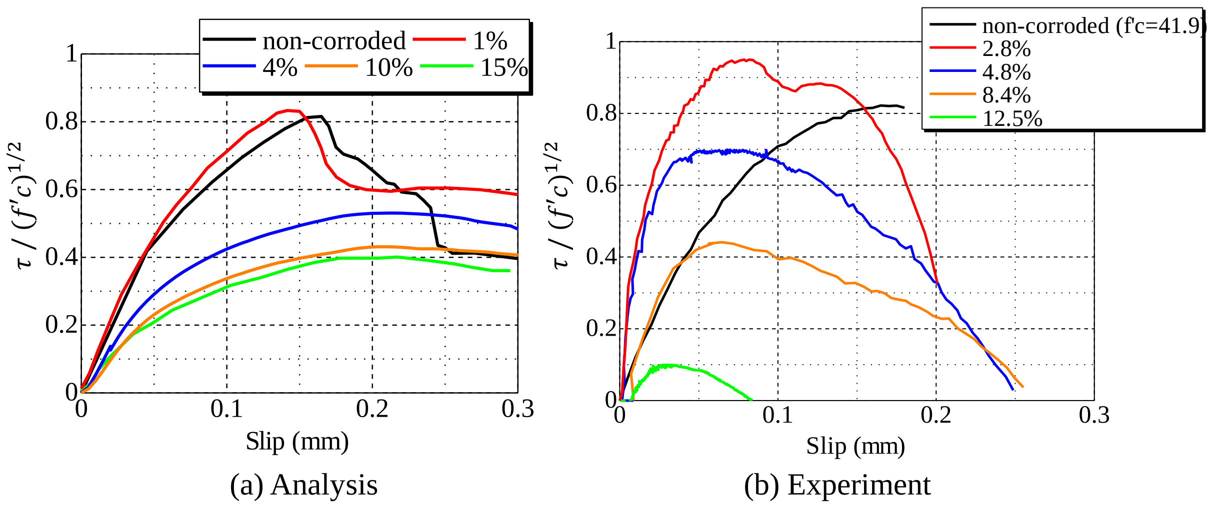

Figure 14 Bond-slip relationship subjected to corrosion of C50 specimen

4.2 Internal crack pattern

Cross-sectional crack patterns at 1/4L of specimen subjected to 1, 4, 15% corrosion are plotted in Figures 15-17. The colors of internal cracks refer to different crack widths. Due to the large differences of crack width under different corrosion degrees, the crack contour shown below has different maximum range. Surface crack width induced by corrosion is also marked in graph. In Figures, corrosion-induced crack obtained from experiment exhibits dependency on concrete cover thickness. With 15mm concrete cover (C/D ratio less than 1.0) two diagonal cracks propagated in concrete cover. On the other hand, with 30 and 50mm concrete cover (C/D ratio greater than 1.0), only one vertical crack propagated in the cover. This dependency coincides with findings in [7,11]. A slower development of surface crack width induced by corrosion with the increase in concrete cover thickness can be captured by analysis. Although a vertical crack can be observed under rebar in 50mm case which is different from test result, the crack width is marginal. It is possibly due to the variation in distribution of corrosion expansion in the experiment. It can be confirmed in both test and numerical analysis that bond failure mode subjected to less than 4% corrosion is the crushing and splitting of concrete near rebar surface, whereas bond failure with larger corrosion degree switches to the splitting of the existing corrosion-induced crack along rebar direction in concrete cover.

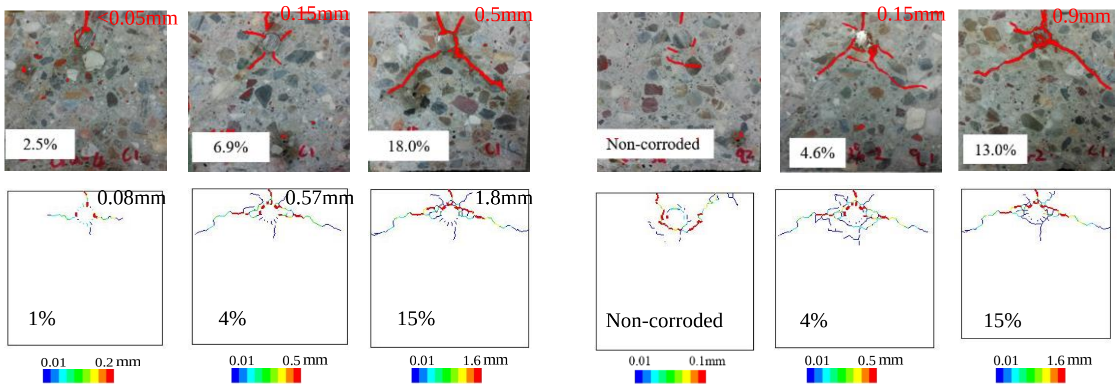

(a) Corrosion-induced crack

(b) Splitting crack due to pull-out

Figure 15 Internal crack pattern of C15 specimen

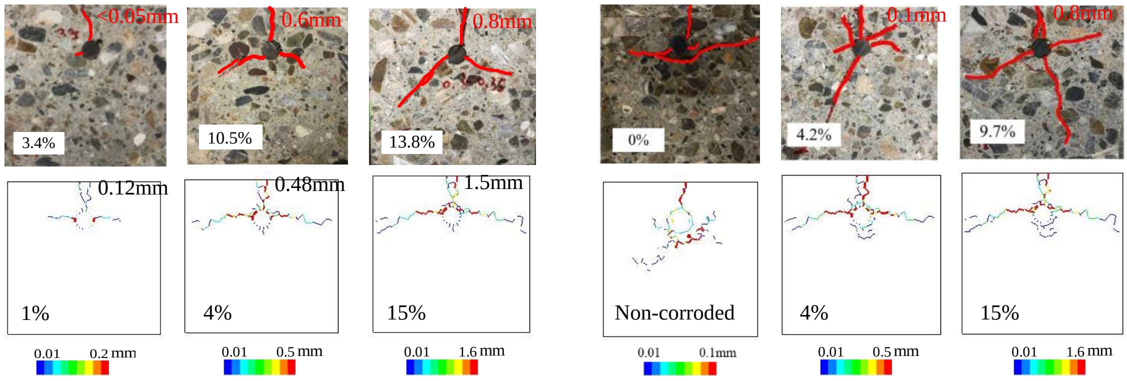

(a) Corrosion-induced crack (b) Splitting crack due to pull-out

Figure 16 Internal crack pattern of C30 specimen

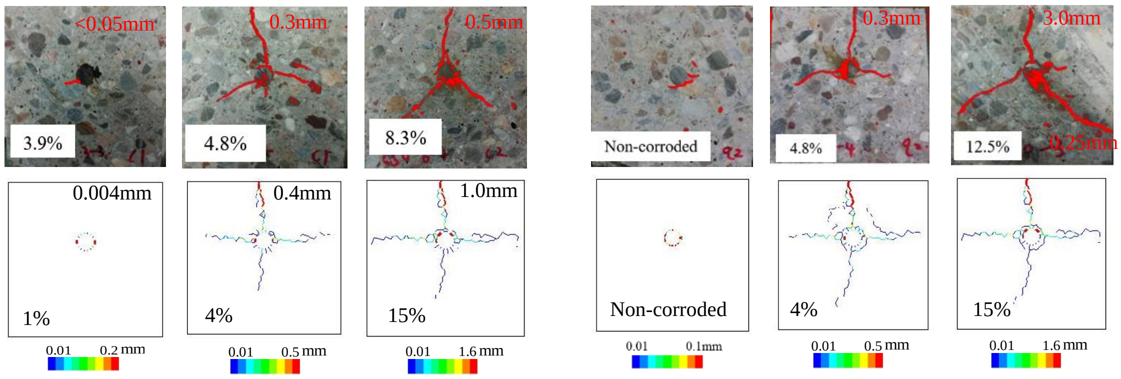

(a) Corrosion-induced crack (b) Splitting crack due to pull-out

Figure 17 Internal crack pattern of C50 specimen

Bond-slip relationship of corroded rebar is resulted from total influences consisting of corrosion-induced crack, corroded rebar shape and rust accumulation, which is closely correlated to the internal crack propagation during rebar pull-out. Therefore, the effect of corrosion-induced crack on surface crack propagation during pull-out by simulation is presented in Figure 18(a). It can be clearly observed from test results in Figure 18(b), as slip initiates, internal splitting cracks generate near rebar surface and propagate towards concrete surface and once surface crack start to propagate, bond-slip curve enters non-linear strengthening stage (see Figure 13). For both analysis and test results, with the increase in corrosion degree, surface crack tends to initiate earlier and develop faster with slip, which is due to the propagation of splitting crack along the corrosion-induced cracks. The analysis shows similar surface crack opening as test results till about 0.15mm slip which corresponds to the slip at ultimate bond strength. It is also observed that crack opening at ultimate bond strength increases with up to 4% corrosion and then gradually decreases. The reason is that surface crack width is firstly widened by the formation of splitting crack along the corrosion crack; while at higher corrosion level due to the large corrosion crack width, confinement of concrete becomes too weak to cause further increment of crack width induced by rebar slippage. Seeing that effects of corroded rebar surface and rust accumulation were not in the focus of this study, certain discrepancies between simulation and experiment can be explained, while a general similar tendency induced by corrosion-induced crack can be understood.

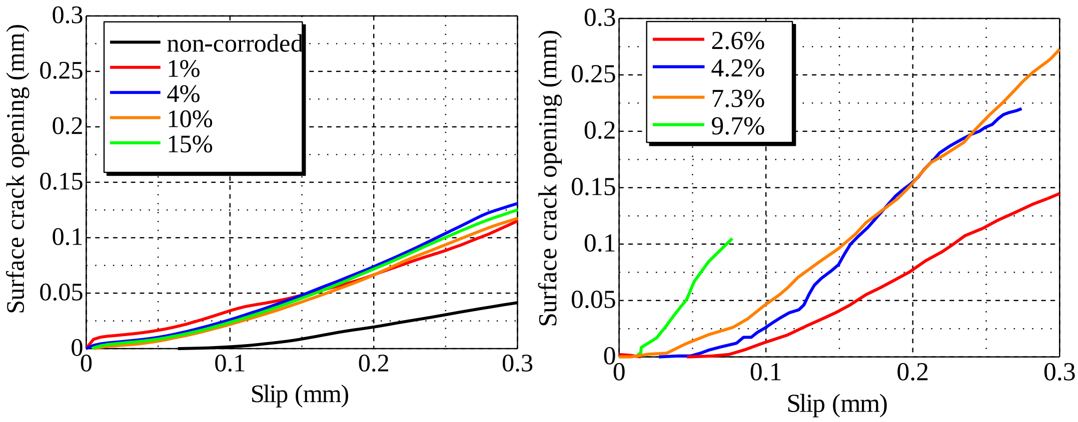

(a) Analysis (b) Experiment

Figure 18 Surface crack opening-slip relationship of C30 specimen

4.3 Ultimate bond strength

Effect of corrosion degree and corrosion crack width on the normalized ultimate bond strength by non-corroded specimen in analysis are summarized and compared with experimental results in Figures 19-20. For all concrete cover cases, under- and over-estimation of normalized bond strength before and after 4 and 10% corrosion compared to the empirical model by Bhargava et al. [36] and experimental results are shown in Figure 19(a). Corresponding to the discussion in section 4.1, this discrepancy is rational since the empirical model and experiment both including the effects of corroded rebar shape and rust accumulation, while the numerical model only considers the influence of corrosion-induced crack. Consequently, the under- and over-estimation amount at small and large corrosion level observed in numerical simulation can be understood. In analysis, bond strength degradation of large concrete cover specimen tends to be slight lager than smaller concrete cover case with same corrosion degree. Moreover, the relationship between normalized bond strength and surface crack width induced by corrosion is further presented in Figure 20. Both numerical and experimental results indicate clear dependency of normalized bond strength on corrosion crack width. Limited degradation could be achieved with crack width larger than 1.0mm. In addition, numerical bond strength tends to decrease faster with corrosion crack width in specimen with larger concrete cover, which coincides with the conclusions led by Banba et al. [37] thought experiment. It proves the conclusion led by previous reports [38-41] that surface crack width is a more practical indicator than corrosion degree during the inspection and evaluation of residual bond strength of the degraded RC members.

As a result, the applicability of the proposed numerical model on considering the single effect of corrosion-induced crack on bond behavior is validated.

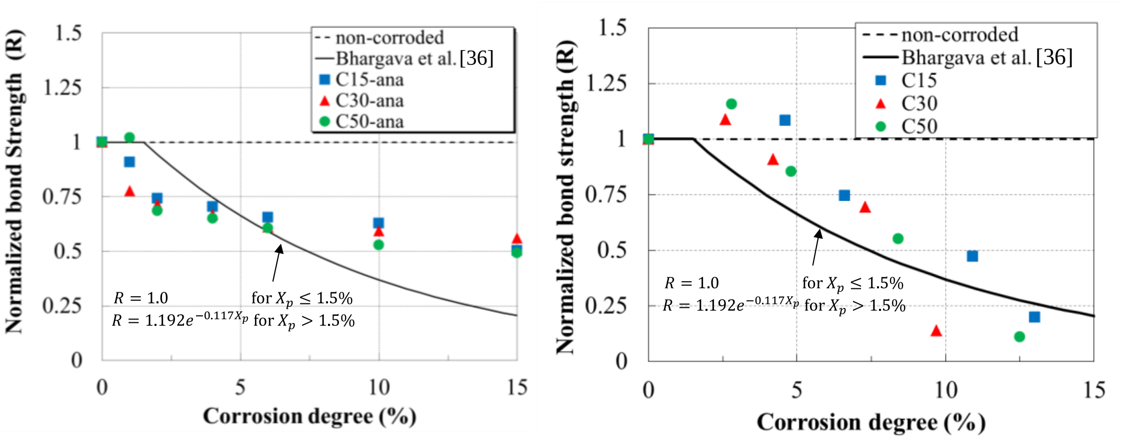

(a) Analysis (b) Experiment

Figure 19 Effect of corrosion degree on ultimate bond strength

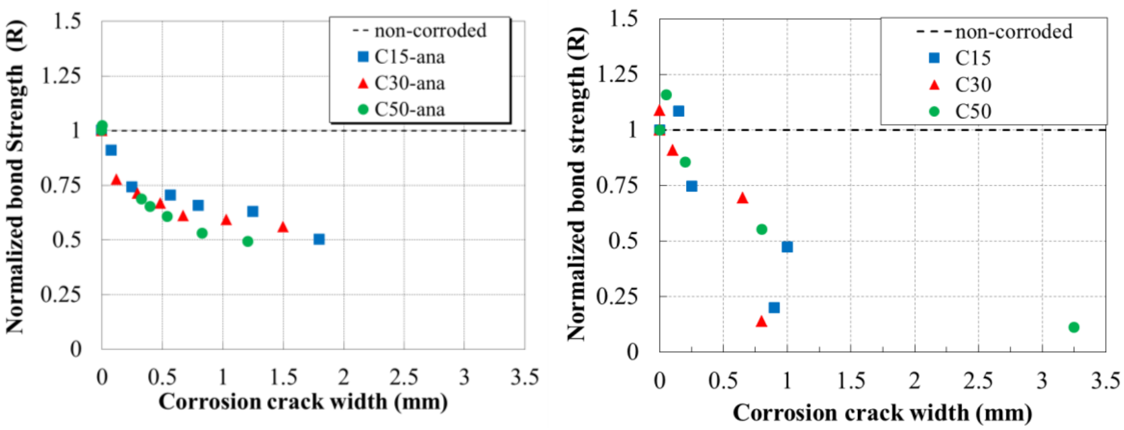

(a) Analysis (b) Experiment

Figure 20 Effect of corrosion crack width on ultimate bond strength

5 Mechanism of bond strength deterioration

Based on the validation of the proposed numerical model to simulate the effect of corrosion-induced crack on bond deterioration, the degradation mechanism with various corrosion-induced cracks is of great importance to be illustrated. Specimens with small difference in cover thickness but distinguished corrosion-induced crack pattern are expected to be compared. Accordingly, 15 and 30mm cover cases are further investigated through the internal crack propagation and stress distribution during pull-out of rebar.

5.1 15mm concrete cover

Figure 21 shows the internal crack propagation in horizontal section at specimen center. In the figure, each crack pattern is corresponding to non-corrosion, 1%, 4% and 15% corrosion cases when slip of rebar becomes 0.05, 0.1, 1.5 and 0.2 mm. Similarly, Figure 22 shows the internal crack at 3/8L cross-section from center perpendicular to the rebar.

For the non-corroded case, as slip reaches to 0.05 mm corresponding to linear stage of bond curve shown in Figure 12(a), the initiation of the micro diagonal crack (Goto's crack) around rebar surface near to rebar ends can be observed (see Figure 21). As slip becomes 0.1 mm, bond-slip enters non-linear stage, crack width near rebar increases accompanied by the development of diagonal cracks leaning towards rebar ends, and the crack propagates towards concrete cover and bottom side of rebar (see Figure 21). Propagation of ring-tension crack in the rebar direction can be observed near to rebar ends as well. After stress reaches to ultimate bond strength at around 0.15 mm slip, propagation of vertical cracks through concrete cover occurs (see Figure 22) followed by the propagation of crack along rebar towards concrete center (see Figure 21). At 0.2 mm slip, the diagonal crack representing shear transfer mechanism from deformed rebar to concrete does not propagate into concrete cover where several vertical cracks propagated, instead, it further develops towards the opposite side of concrete cover (see Figure 21).

On the other hand, due to the existence of corrosion-induced cracks in the direction of concrete cover before the rebar was pulled out, the propagation of diagonal cracks into concrete cover can barely be observed (see Figure 22). Hence, cross-sectional crack pattern subjected to rebar pull-out shown is consistent as corrosion-induced crack, while only crack width is enhanced. In addition, on the opposite side of concrete cover, the propagation level of diagonal crack is much smaller compared to non-corroded specimen (see Figure 21). Consequently, with the existence of corrosion-induced crack in concrete, the propagation of diagonal crack generated during pull-out test is suppressed.

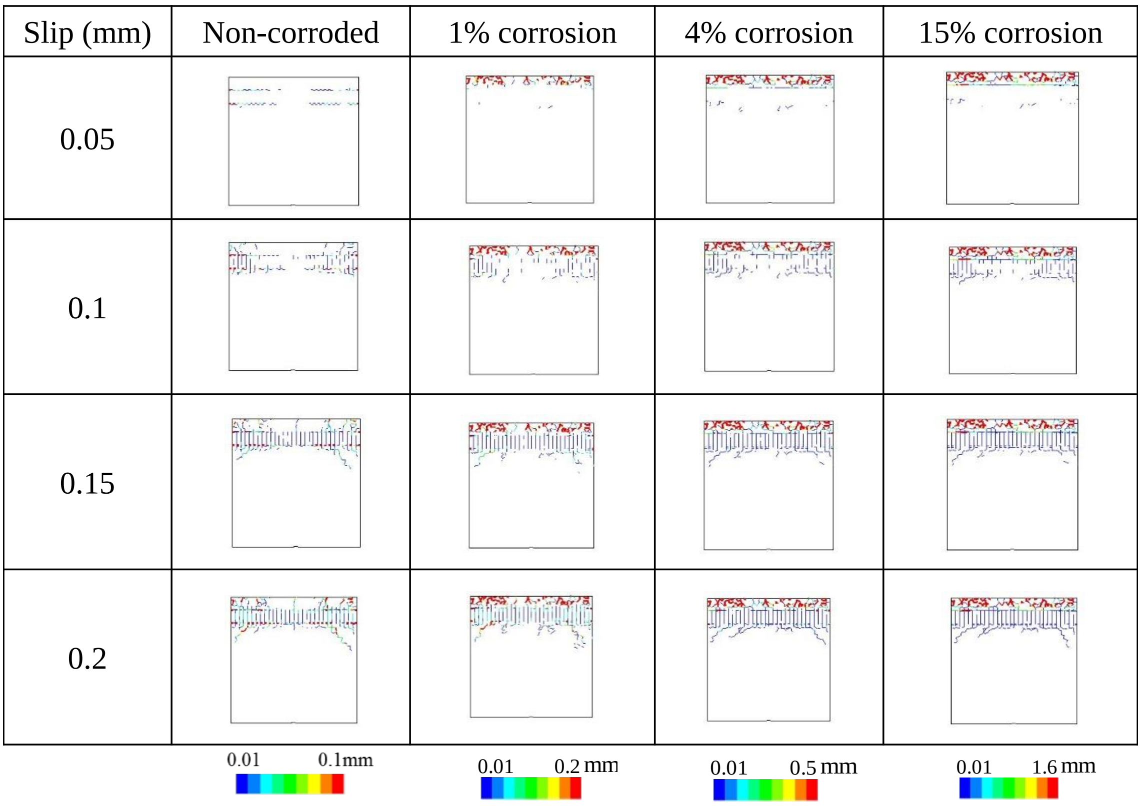

Figure 21 Internal crack pattern at horizontal cross-section of C15 specimen

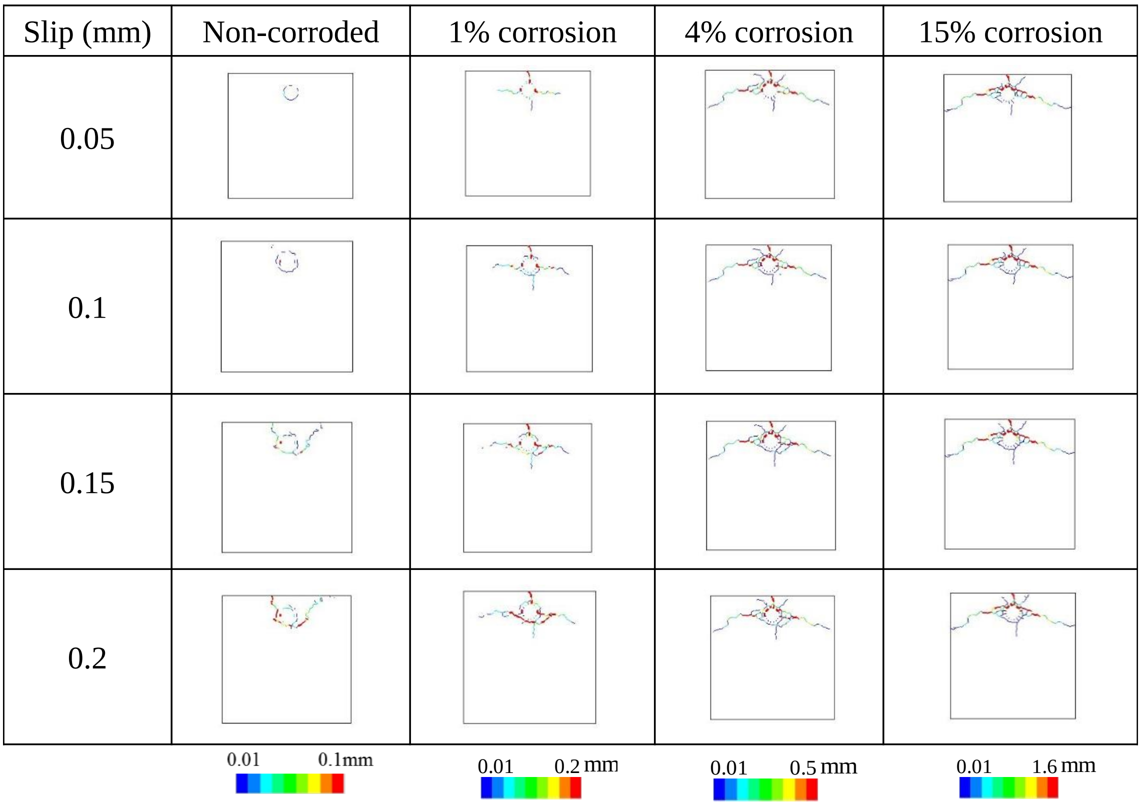

Figure 22 Internal crack pattern at 3/8L cross-section of C15 specimen

Corresponding to internal crack propagation, internal normal stress distribution of concrete along rebar direction at horizontal and 3/8L cross-section are plotted in Figures 23-24. Considering the rebar stress is much larger than the stress in concrete, the range of stress contour is set within 2.69MPa (tensile strength of concrete) to -5.0MPa (compression) to only consider the stress status in the concrete.

For the non-corroded case at 0.05 mm slip, in Figure 23, tensile stress in rebar direction distributes evenly around rebar and marginal compressive stress distributes at rebar ends where micro diagonal cracks generated in Figure 21. As slip increases to 0.1 mm, the formation of diagonal compression struts near rebar surface and enhanced tensile stress at specimen center can be obtained (see Figures 23-24). Compression struts is formed between the propagated diagonal cracks induced by the cumulative compression and ring-tension around rebar. It plays an essential role in the bond mechanism of deformed rebar and concrete according to [34]. When slip continues to increase till 0.15mm, area and magnitude of compression struts improves with development of diagonal crack (see Figures 23-24), resulting in the non-linear strengthening stage of bond stress in Figure 12(a). As slip reaches to 0.15mm, concentration of tensile stress in specimen center causes the splitting of concrete cover and once splitting crack appears, tensile stress vanished in concrete cover and compressive stress redistribute on the opposite side of concrete cover (see Figure 23). As a result, the ultimate bond strength is achieved. When slip approaches 0.2 mm, limited degradation of compressive stress in compression struts is illustrated (see Figures 23-24), thus ductile softening failure is captured in bond-slip relationship in Figure 12.

With the existence of corrosion-induced crack, tensile and compressive stress is barely generated in concrete cover and area and magnitude of distribution on the opposite side is clearly degraded compared to non-corroded case at each slip (see Figures 23-24). As a result, new splitting crack does not generate in concrete cover as shown in both analysis and test results and propagation of diagonal cracks at rebar bottom is largely suppressed in Figure 22. Consequently, the deteriorated cumulative effect of compression struts and ring-tension is unable to transfer the stress in shear springs on interface elements to surrounding concrete.

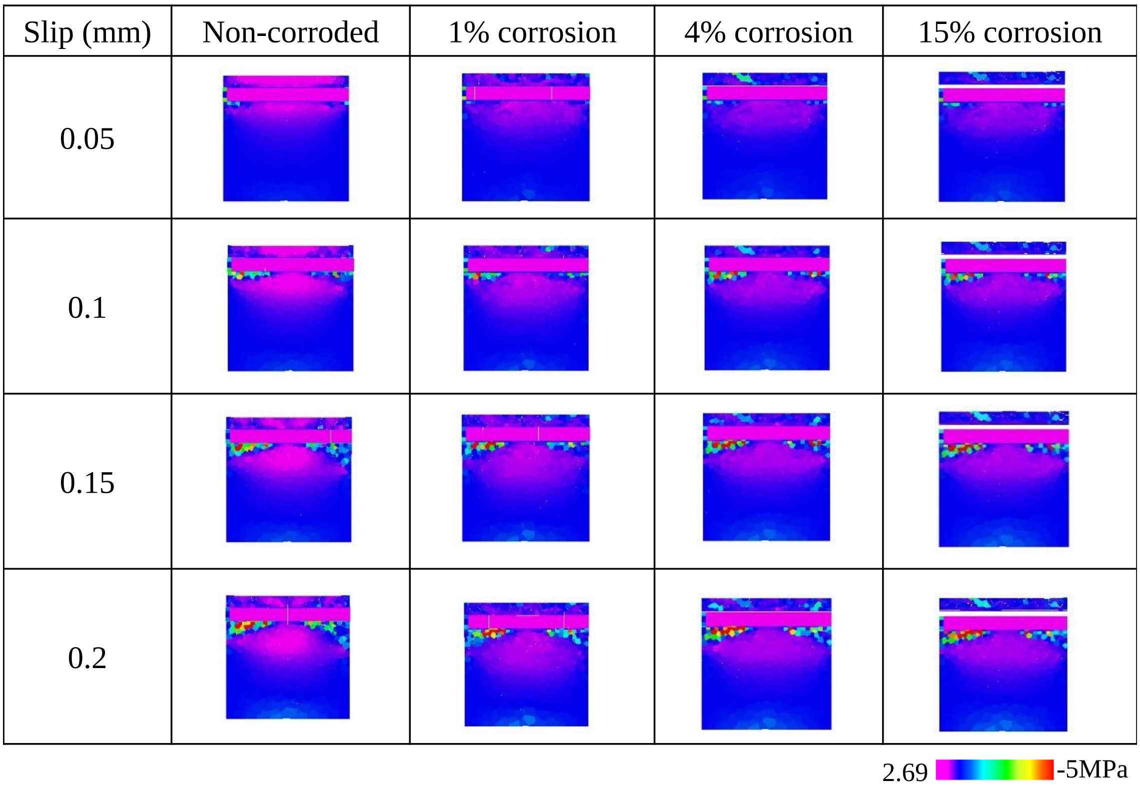

Figure 23 Internal stress distribution at horizontal cross-section of C15 specimen

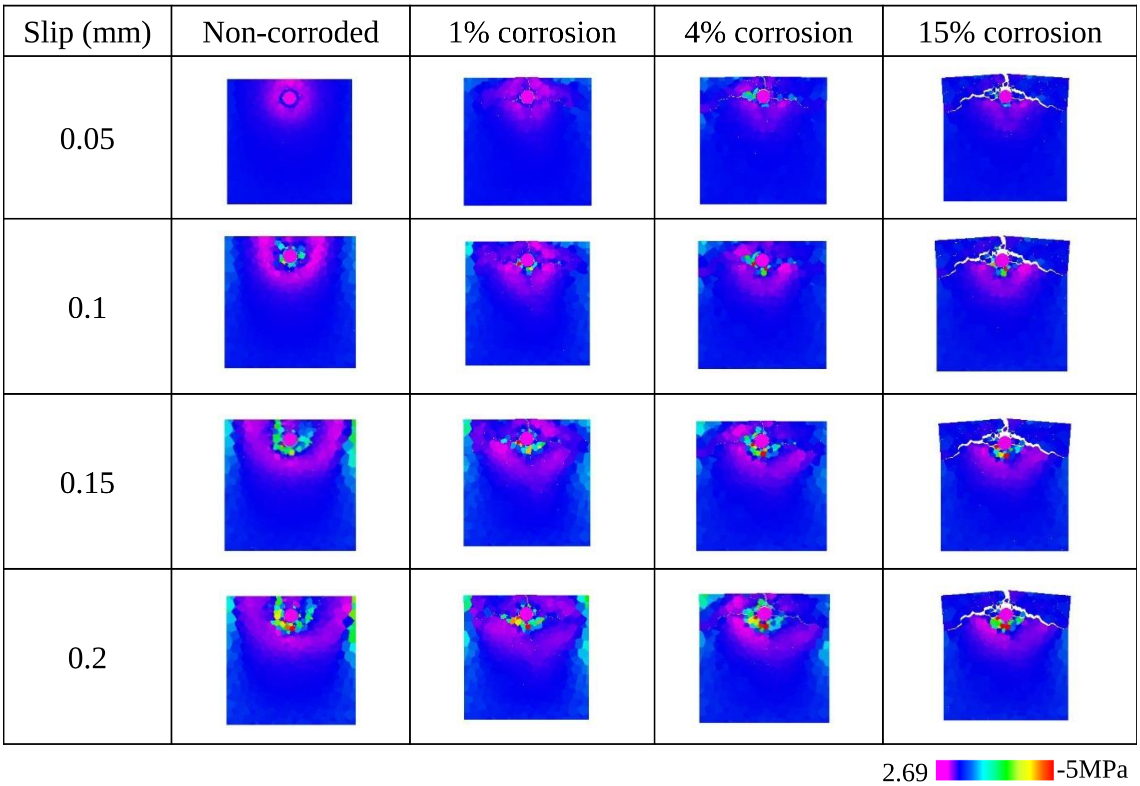

Figure 24 Internal stress distribution at 3/8L cross-section of C15 specimen

5.2 30mm concrete cover

In comparison to specimen with 15mm concrete cover, Figures 25-26 shows the internal crack propagation of specimen with 30mm concrete cover. For the non-corroded case, the generation of micro diagonal cracks from two ends is observed in Figure 25 as 15mm specimen. As slip increase from 0.1mm to 0.15mm, ultimate bond strength is reached (see Figure 13(a)) and the propagation of splitting crack in concrete cover (see Figure 26) and diagonal cracks at rebar bottom (see Figure 25) is confirmed. Propagated length and number of the splitting and diagonal cracks is more pronounced than specimen with smaller concrete cover shown in Figure 21.

With the increase of corrosion degree, generation of splitting crack in the concrete cover is suppressed by the existing corrosion cracks (see Figure 26); diagonal cracks in the opposite side are largely affected (see Figure 25). Compared to specimen with fewer concrete cover in Figure 22, rebar slippage exert fewer newly generated crack in concrete cover, which only cause the splitting of concrete cover along the existing corrosion-induced crack.

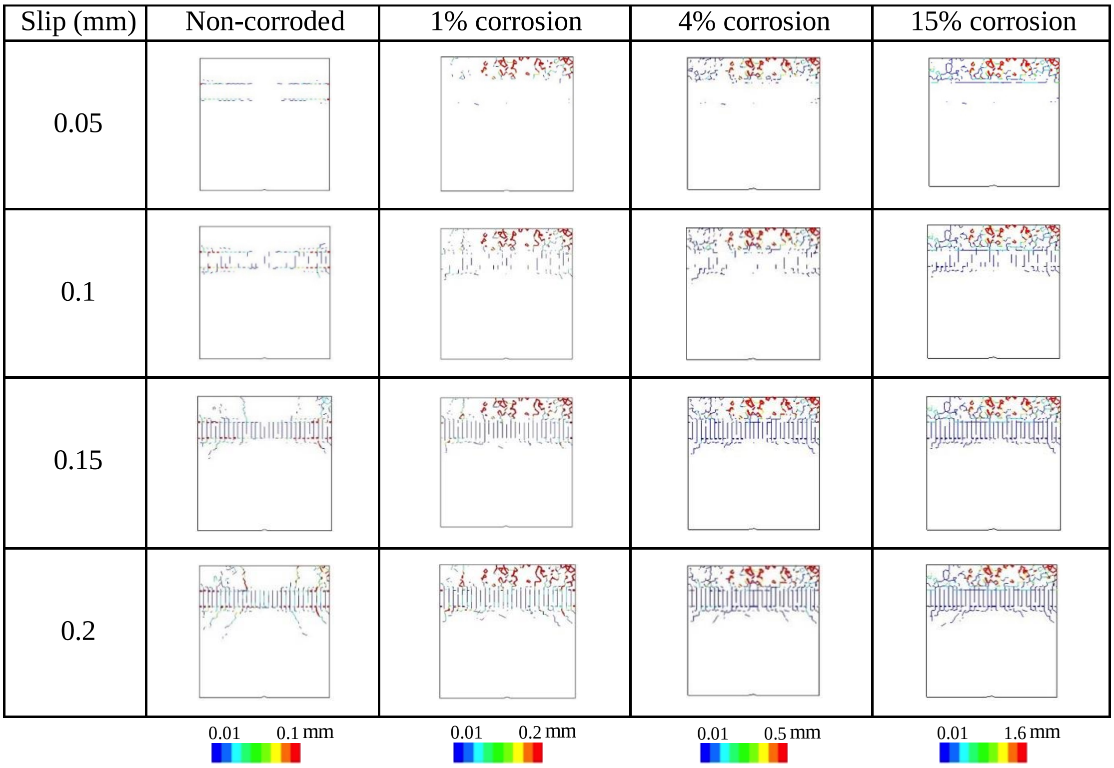

Figure 25 Internal crack pattern at horizontal cross-section of C30 specimen

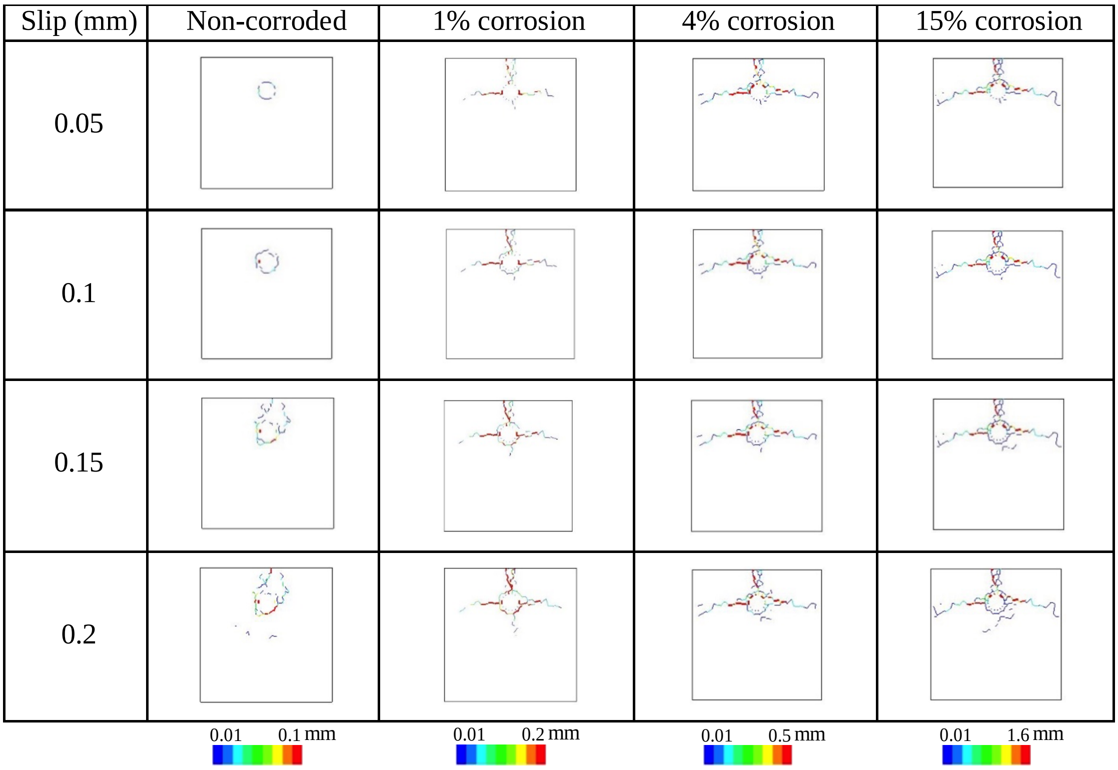

Figure 26 Internal crack pattern at 3/8L cross-section of C30 specimen

Correspondingly, horizontal and cross-sectional internal stress distribution of concrete is shown in Figures 27-28.

For the non-corroded case as rebar slip increase from 0.05 to 0.2mm, it is clearly shown in Figures 27-28 that the distribution area and magnitude of compressive and tensile stress is larger than specimen with smaller concrete cover, which correlates to a higher bond stress. In the softening stage as slip larger than 0.2mm, the redistribution of diagonal compression struts towards the opposite side of concrete cover is more significant than smaller concrete cover case. Consequently, a more brittle softening segment in bond-slip curve is obtained (see Figure 13).

Comparably, with the appearance of corrosion-induced crack in concrete cover up to 4% corrosion (see Figure 26), tensile stress in concrete cover drastically reduces and compression struts redistribute on the opposite side of concrete cover with higher stress level, though some compressive and tensile stress still retained in the cover (see Figures 27-28). Compared to specimen with smaller concrete cover, both area and magnitude of compressive stress around rebar is more pronounced, which allows relative higher bond in specimen with larger concrete cover at same corrosion degree. At 15% corrosion normalized bond strength is similar among the different cover thickness, whereas the thicker the cover, the smaller the surface crack width and vice versa (see Figure 20(a)). Although corrosion crack width is smaller and crack number is fewer in larger concrete cover case, larger distribution area of stress is likely to be affected. Hence it is verified that bond behavior of specimen with larger cover thickness is more sensitive to the corrosion-induced crack.

From above discussion, it has been clarified that the combined effects of degradation of the compressive stress in diagonal compression struts and ring-tension around rebar induced by corrosion-induced crack, contribute to the degradation of ultimate bond strength.

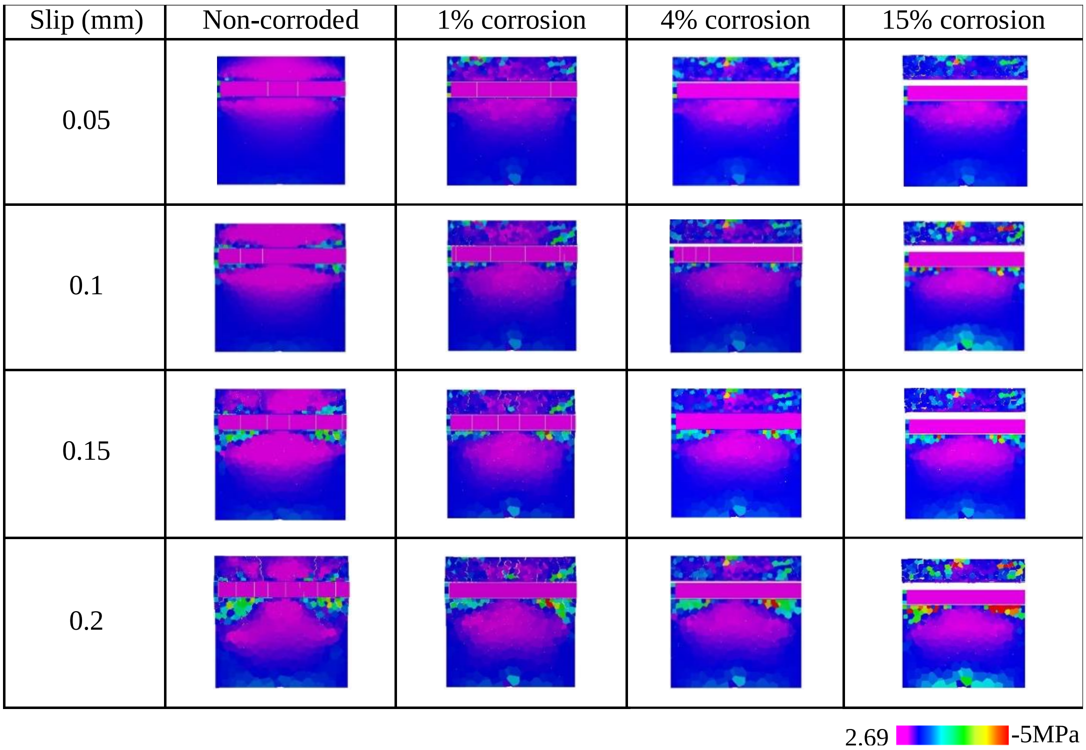

Figure 27 Internal stress distribution at horizontal cross-section of C30 specimen

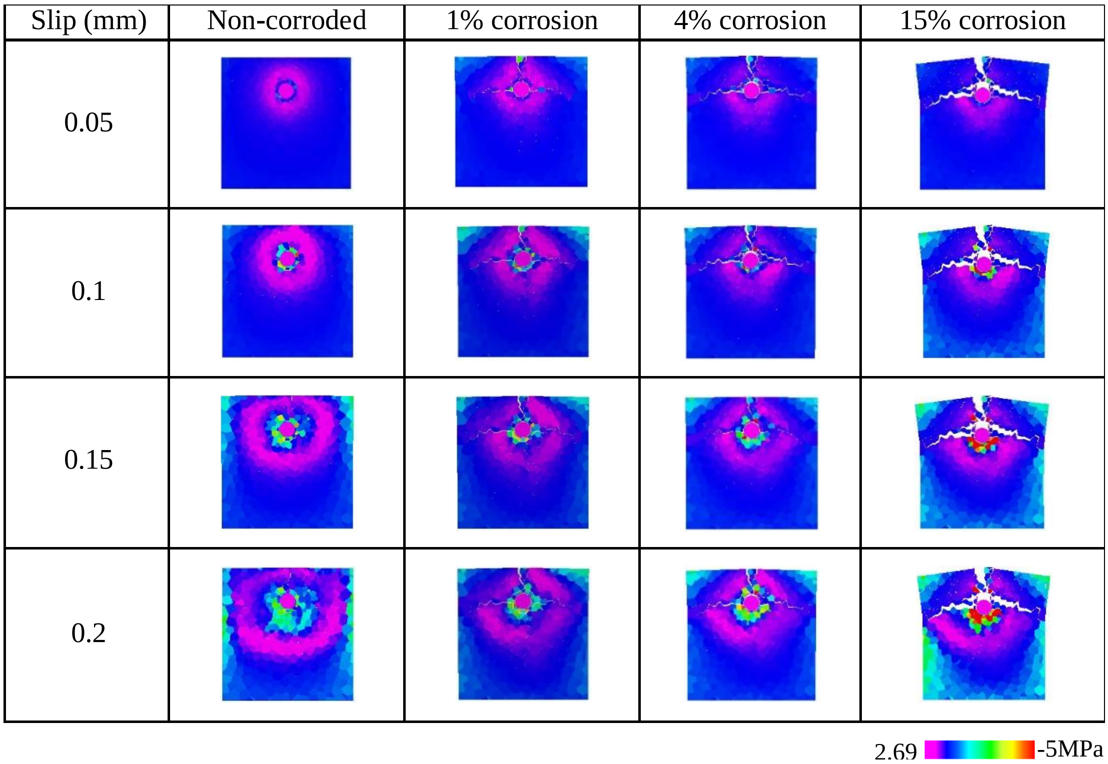

Figure 28 Internal stress distribution at 3/8L cross-section of C30 specimen

6 Conclusions

Following conclusions were derived from this study:

1. A numerical method based on 3D RBSM was developed to simulate corrosion-induced crack and bond behavior in which the rebar was modeled by solid elements without explicit geometry of rebar ribs. This simplified model is able to consider the corrosion expansion and shear transfer by interface element.
2. Proposed numerical model has been validated to obtain reasonable simulation accuracy of non-corroded specimen similar to meso-scale model with high modeling conciseness and computational efficiency.
3. The proposed model is able to reproduce the bond deterioration subjected to corrosion-induced crack considering concrete cover thickness.

4. The corrosion crack width was confirmed to be a good indicator of bond strength degradation subjected to various concrete cover.
5. Bond deterioration mechanism induced by corrosion-induced crack was found to be combined effects of degradation of the compressive stress in diagonal compression struts and ring-tension around rebar. Bond deterioration of specimen with larger concrete cover is more sensitive to formation of corrosion-induced crack.

Acknowledgment

The research presented in this work was conducted at Nagoya University.

References

[1] Rodriguez, J., Ortega, L. M., Casal, J., (1997). "Load carrying capacity of concrete structures with corroded reinforcement". Construction and Building Materials, 11, 239-248.

[2] Mangat, P. and Elgarf, M., (1999). "Flexural strength of concrete beams with corroding reinforcement". ACI Structural Journal, 96, 149-158.

[3] Yoon, S. C., Wang, K. J., Weiss, W. And Shah, S., (2000). "Interaction between loading, corrosion, and serviceability of reinforced concrete". ACI materials Journal, 97(6), 637-644.

[4] El Maaddawy, T., Soudki, K., Topper, T., (2005). "Long-term performance of corrosion-damaged reinforced concrete beams". ACI Structural Journal, 102(5), 649-656.

[5] Yang, Y., Nakamura, H., Miura, T., Yamamoto, Y., (2019). "Effect of corrosion-induced crack and corroded rebar shape on bond behavior". Structural Concrete, 20(6), 2171-2182.

[6] Bazant, Z.P., (1979). "Physical model for steel corrosion in concrete sea structures-Theory". Journal of the Structural Division, Proceedings of the ASCE, 105(ST6), 1137-1153.

[7] Tsutsumi, T., Matsushima, M., Murakami, Y., Seki, H., (1996). "Study on crack models caused by pressure due to corrosion products". Doboku Gakkai Ronbunshuu, 30(2), 159-166. [in Japanese]

[8] Cabrera, J. G., (1996). "Deterioration of Concrete Due to Reinforcement Steel Corrosion". Cement and Concrete Composites, 18, 47-59.

[9] Care, S., Nguyen, Q.T., Beddiar, K., Berthaud, Y., (2010). "Times to cracking in reinforced mortar beams subjected to accelerated corrosion tests". Materials and Structures, 43, 107-124.

[10] Nakamura, H., Tran, K.K., Kawamura, K., Kunieda, M., (2010). "Crack propagation analysis due to rebar corrosion". Proceedings of the 7th International Conference on Fracture Mechanics of Concrete and Concrete Structures (FramCoS-7), Korea, 921-928.

[11] Qiao, D., Nakamura, H., Yamamoto, Y., Miura, T., (2016). "Crack patterns of concrete with a single rebar subjected to non-uniform and localized corrosion". Construction and Building Materials, 116, 366-377.

[12] Alonso, C., Andrade, C., Rodriguez, J., Diez, J.M., (1998). "Factors controlling cracking of concrete affected by reinforcement corrosion". Materials and Structures, 31, 435-441.

[13] Vidal, T., Castel, A., Francois, R., (2004). “Analyzing crack width to predict corrosion in reinforced concrete”. Cem. Concr. Res., 34(1), 165-174.

[14] Lee, H. S., Noguchi, T., Tomosawa, F., (2002). “Evaluation of the bond properties between concrete and reinforcement as a function of the degree of reinforcement corrosion”. Cement and Concrete Research, 32, 1313-1318.

[15] Lundgren, K., (2002). “Modelling the effect of corrosion on bond in reinforced concrete”. Magazine of Concrete Research, 54(3), 165-173.

[16] Berra, M., Castellani, A., Coronelli, D., Zanni, S., Zhang, G., (2003). “Steel-concrete bond deterioration due to corrosion: finite-element analysis for different confinement levels”. Magazine of Concrete Research, 55(3), 237-247.

[17] Amleh, L. and Ghosh, A., (2006). “Modeling the effect of corrosion on bond strength at the steel-concrete interface with finite-element analysis”. Can. J. Civ. Eng., 33, 673-682.

[18] Hanjari, K. Z., Lundgren, K., Plos, M., Coronelli, D., (2013). “Three-dimensional modelling of structural effects of corroding steel reinforcement in concrete”. Structure and Infrastructure Engineering, 9(7), 702-718.

[19] Lundgren, K., (2007). “Effect of corrosion on the bond between steel and concrete: an overview”. Magazine of Concrete Research, 59(6), 447-461.

[20] Ozbolt, J., Orsanic, F., Balabanic, G., (2014). “Modeling pull-out resistance of corroded reinforcement in concrete: Coupled three-dimensional finite element model”. Cement and Concrete Composites, 46, 41-55.

[21] Jiradilok, P., Nagai, K., Matsumoto, K., (2019). “Meso-scale modeling of non-uniformly corroded reinforced concrete using 3D discrete analysis”. Eng. Struct., 197, 109378.

[22] Jiradilok, P., Wang, Y., Nagai, K., Matsumoto, K., (2020). "Development of discrete meso-scale bond model for corrosion damage at steel-concrete interface based on tests with/without concrete damage". Construction and Building Materials, 236.

[23] Yamamoto, Y., Nakamura, H., Kuroda, I., Furuya, N., (2014). "Crack propagation analysis of reinforced concrete wall under cyclic loading using RBSM". European Journal of Environmental and Civil Engineering, 18(7), 780-792.

[24] Tran, K.K., Nakamura, H., Kawamura, K., Kunieda, M., (2011). "Analysis of crack propagation due to rebar corrosion using RBSM". Cement and Concrete Composites, 33, 906-917.

[25] Qiao, D., Nakamura, H., Yamamoto, Y., Miura, T., (2016). "Modeling of corrosion-induced damage in reinforced concrete considering electro-mechanical coupling". Journal of Advanced Concrete Technology, 14, 664-678.

[26] Amalia, Z., Nakamura, H., Miura, T., Yamamoto, Y., (2018). "Development of simulation method of concrete cracking behavior and corrosion products movement due to rebar corrosion". Construction and Building Materials, 190, 560-572.

[27] Cairns, J. and Abdullah, R.B., (1996). "Bond strength of black and epoxy-coated reinforcement—a theoretical approach". ACI Mater. J., 93(4), 362–369.

[28] Coronelli, D., (2002). "Corrosion cracking and bond strength modeling for corroded bars in reinforced concrete". ACI Struc. J., 99(3), 267-276.

[29] Coccia, S., Imperatore, S., Rinaldi, Z., (2016). "Influence of corrosion on the bond strength of steel rebars in concrete". Materials and Structures, 49, 537-551.

[30] Comite Euro-International du Beton, (1990). CEB-FIP Model code 1990, First draft. Paris: CEB.

[31] ACI., (1992). Building Code Requirements for Reinforced Concrete, 318-377.

[32] Iizuka, K., Higai T., Saito, S., Takahashi, R., (2011). "Bond stress-slip-strain relationship of deformed bars including the effect of concrete cover thickness". Journal of JSCE, 67, 280-296. [in Japanese]

[33] Ikuma, K., Yamamoto, Y., Nakamura, H., Miura, T., (2018). "Mesoscale simulation of bond behavior of deformed rebar based on coupled RBSM-FEM method". Proceedings of JCI annual convention, 40, 541-546. [in Japanese]

[34] Goto, Y., (1971). "Cracks formed in concrete around deformed tension bars". ACI Journal, 68, 244-251.

[35] Desnerck, P., Lees, J., Morley, C., (2015). "Bond behavior of reinforcing bars in cracked concrete". Construction and Building Materials, 94, 126-136.

[36] Bhargava, K., Ghosh, A. K., Mori, Y., Ramanujam, S., (2007). "Corrosion-induced bond strength degradation in reinforced concrete-Analytical and empirical models". Nuclear Engineering and Design, 237, 1140-1157.

[37] Banba, S., Abe, T., Nagaoka, K., Murakami, Y., (2014). "Evaluation method for bond-splitting behavior of reinforced concrete with corrosion based on confinement stress of concrete against corrosion expansion". Journal of Advanced Concrete Technology, 12, 7-23.

[38] Cairns J., Du Y., Law D., (2006). "Residual bond strength of corroded plain round bars". Magazine of concrete research, 58(4), 221-231.

[39] Law, D. W. and Tang, D., (2011). "Impact of crack width on bond: confined and unconfined rebar". Materials and Structures, 44, 1287-1296.

[40] Fisher C. and Ozbolt J., (2012). “Influence of bar diameter and concrete cover on bond degradation due to corrosion in: J. Cairns, G. Metelli, G. Plizzari, (Eds)”. Proceeding of 4th international symposium: Bond in Concrete 2012: Bond, Anchorages, Detailing, 17-20 June 2012, Brescia, Italy.

[41] Mak M.W.T., Desnerck P., Lees J.M., (2019). “Corrosion-induced crack and bond strength in reinforced concrete”. Construction and Building Materials, 208, 228-241.